Study of the Multipactor Effect in Ridge Gap Waveguide Technology

Sarah M. Bonte [(1)], Manuel Sancho [(1)], Angela Coves [(1)], Eva Rajo[(2)], José Joaquín Vague[(3)], and Vicente E. Boria [(3)]

[(1)] Departamento de Ingeniería de Comunicaciones – I3E
Universidad Miguel Hernández de Elche, 03202 Elche, Spain
Email: sbonte@umh.es, manuel.sancho@goumh.umh.es, angela.coves@umh.es

[(2)] Department of Signal Theory and Communication
University Carlos III of Madrid, 28911 Madrid, Spain
Email: eva.rajo@uc3m.es

[(3)] Departamento de Comunicaciones - ITEAM
Universidad Politècnica de València, 46022 Valencia, Spain
Email: jvague@dcom.upv.es, vboria@dcom.upv.es

ABSTRACT

Multipactor is an undesired high-power effect that frequently occurs under high-vacuum conditions in microwave and millimeter-wave components. These components are used in a wide range of different scenarios, such as satellite communication payloads, traveling-wave tubes, as well as particle accelerators. When in a high-vacuum environment, the free electrons, that are inside the device, are accelerated by the electromagnetic fields operating at radio frequency (RF), and they impact against the metallic walls. Then, more secondary electrons are released, giving rise to an avalanche of electrons, and producing a resonant discharge inside the affected component with many adverse consequences. Among them, we find detuning of resonant cavities, power dissipation, a significant increase of noise in communication systems, and even physical damage in the component involved. While multipactor susceptibility has been extensively studied in conventional waveguides, its impact on other guided technologies, such as Ridge Gap Waveguides (RGWs), remains largely unexplored.

The ridge gap waveguide technology has emerged as a promising one for high-frequency applications and components (i.e. filters), due to their low-loss characteristics and compatibility with standard fabrication processes. In this article, the power threshold level (related to the multipactor effect) within ridge gap waveguides is studied, focusing on understanding the distribution and propagation of electromagnetic energy along this waveguide structure. Through simulations, the dependence of multipactor threshold levels on various parameters, such as the ridge dimensions and its proximity to the bed of pins is studied. The insights provided in this research, will help with the future design and implementation of efficient and reliable high-frequency communication and sensing systems for space applications utilizing ridge gap waveguide technology.

I. INTRODUCTION

Multipactor is a well-known and undesired high-power effect frequently observed in microwave and millimeter-wave components operating under high-vacuum conditions [1], which are used in a wide range of different scenarios, such as satellite communication payloads, traveling-wave tubes, as well as particle accelerators. In an ultra-high vacuum environment, the free electrons inside the microwave component are accelerated by the radio frequency (RF) electromagnetic fields, impacting against its metallic walls and releasing more secondary electrons, giving rise to an avalanche of electrons. Thus, a resonant discharge is produced inside the affected component with a large number of adverse consequences [2]. Among them, it is worth mentioning the detuning of resonant cavities, power dissipation, a significant increase of noise in communication systems, and even physical damages in the involved component.

Over the years, multipactor susceptibility charts for parallel-plate waveguides have been developed using both analytical models [3] and empirical data [4]. The charts are used for approximate prediction of the multipactor power threshold in different microwave components, either metallic or including dielectric materials [5], [6]. More recently, the multipactor effect has been explored in a broader range of waveguides and transmission lines, including rectangular [7] – [10], circular [11], elliptical [12], and coaxial waveguides [13], [14], as well as planar microstrip lines [15]. There is also a recent work on multipactor effect in Groove Gap Waveguide (GGW) technology [16], a very promising alternative to Rectangular Waveguide (RW) technology, due to its potential advantages, because perfect metallic contact between its different parts (top cover and body) is not needed [17], [18]. Therefore, it is a good alternative to replace the standard hollow RW in high-frequency components.

Another promising gap waveguide variant is the Ridge Gap Waveguide (RGW) [19], [20] which has become a very useful transmission solution for high-frequency applications, because of its intrinsic low-loss properties and

seamless integration into standard fabrication processes. This type of waveguide has been used for the development of efficient and reliable high-frequency communication and sensing systems, especially due to its compact size that makes it ideal for the design of feeding networks and beamforming networks in antenna systems [21]-[23]. Despite the growing use of RGWs in high-frequency applications, to the authors' knowledge, no contribution has been devoted to the study of multipactor discharge breakdown in this technology, which is necessary to fully harness its potential to be used in space applications.

This article presents a theoretical and experimental study of the multipactor threshold levels in RGW technology. Through rigorous simulations, the dependence of power levels on various parameters such as the ridge dimensions and its proximity to the bed of pins is explored. Next, in order to validate the previous theoretical study, an E-plane WR-51 waveguide transformer, where the central section is implemented in RGW, is designed to be manufactured in aluminium. Finally, the multipactor threshold levels of this transformer have been simulated and will be measured in a near future, for validation purposes.

II. GEOMETRY AND INITIAL DESIGN

The geometry of the Ridge Gap Waveguide (RGW) under study can be seen in Fig. 1(a) (3D view) and (b) (cross section), respectively. It is characterized by having a ridge in the central area where the electromagnetic fields will propagate, and beds of pins arranged following a spatial periodicity d. The periodic pins are inserted in the RGW body to provide a high-impedance boundary condition to the top lid (where a small gap of height H_A between the pins and the top lid is present). Thus, a perfect metallic contact between the top lid and the body is not needed anymore [16], [18]. The RGW has been initially designed to operate between 17 GHz and 18 GHz (in K-band). This frequency range is chosen according to the RF power availability in the facility where multipactor validation tests are aimed to be performed, i.e., the High Power RF Space Laboratory of the European Space Agency (ESA) and the Val Space Consortium (VSC) [24]. It is important to note that the validated multipactor study can be directly scaled up to higher frequency bands, where RGW is a very promising technological solution.

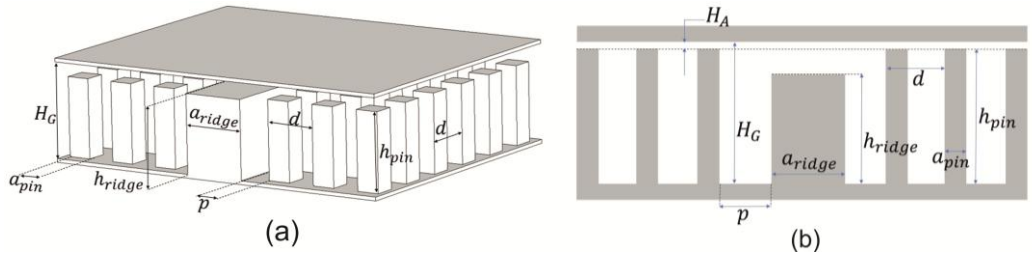

Fig. 1. Geometry of the RGW under study. (a) 3D view and (b) cross-section of the RGW.

The selected initial dimensions must ensure a good frequency response, i.e., single-mode propagation from 17 GHz to 18 GHz, and a multipactor power level below 7 kW (maximum power level that can be measured in the cited laboratory). The simulations have been performed with the commercial software tool CST Studio Suite, (v. 2023, Dassault Systèmes) [25], which allows us to obtain the dispersion diagram and electromagnetic fields of the waveguide under study, and with SPARK3D (v. 2023, Dassault Systèmes). The latter one is a multipactor simulation tool that uses the computed electromagnetic fields in the component for driving charged particles (electrons). Taking into account the previous considerations, and after some iterations, we obtained the following initial RGW dimensions: a_{ridge} = 3 mm, h_{ridge} = 5.38 mm, H_A = 1.1 mm. Regarding the periodic bed of pins (of square cross-section with side a_{pin} and height h_{pin}, periodicity d and a separation p of the ridge to the first pin, see Fig. 1), it has been properly designed to implement the high-impedance surface of the RGW technology, thus obtaining p = 1.1625 mm, d = 3.25 mm, a_{pin} = 1.5 mm, h_{pin} = 5.38 mm. Note that in this initial design, the same height has been chosen for the ridge and pins, since in most existing circuits using RGW, the height of the ridge is chosen to be identical to that of the pins.

The dispersion diagrams for this initial periodic bed of pins and the corresponding RGW are presented in Fig. 2, where Fig. 2(a) displays the dispersion diagram for the pin unit cell, and Fig. 2(b) shows the dispersion diagram for the RGW unit cell. In Fig. 2(b), the unwanted modes are depicted in blue, while the RGW mode is shown in red. The monomode operational bandwidth has been highlighted in grey, which ranges from approximately 11 GHz to 21 GHz.

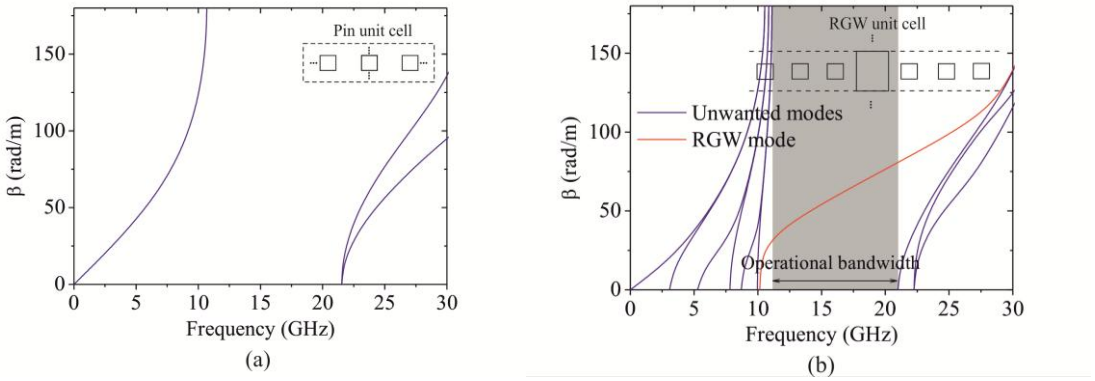

Fig. 2. Dispersion diagram of (a) the pin unit cell and (b) the RGW unit cell.

Next, we will examine the region where the electromagnetic (EM) fields are more intense, and thus, more susceptible for an electron discharge to occur. For this initial design, the distribution of the electric field magnitude along the RGW geometry design has been computed at 17.5 GHz, and it is displayed in Fig. 3. For simplicity, ohmic losses have not been considered in this initial design, i.e. we have considered PEC in the metallic parts. As can be observed, the maximum field intensity is clearly located over the ridge and not above the metallic pins, as expected. Nevertheless, for the parametric study of the multipactor (MP) power threshold P_{TH} of such a waveguide as a function of its various parameters, to be performed in section 3, the monomode regime of the RGW will always be checked, as well as ensuring that the region of maximum EM field is located over the ridge.

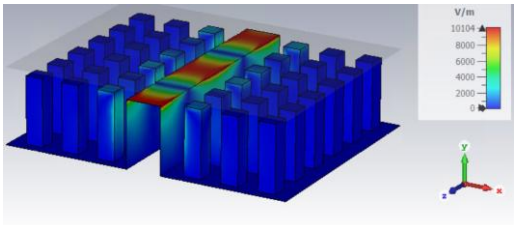

Fig. 3. Electric field distribution in the RGW with geometrical parameters used in Fig. 2.

Furthermore, by reducing the ridge height, a study was performed to investigate how the electromagnetic field distribution changes and to evaluate the effect on the cutoff frequency. Table 1 shows the variation of the cutoff frequency of the RGW with the ridge height. The results show that even with a reduced ridge height, the electromagnetic fields continue to be concentrated on the ridge, unlike in the groove gap waveguide case (where the higher electric field levels are shifted to the first pins [16]), despite the cutoff frequency being close to the considered frequency of 17.5 GHz. This is shown in Fig. 4, where the ridge height is reduced to 3 mm.

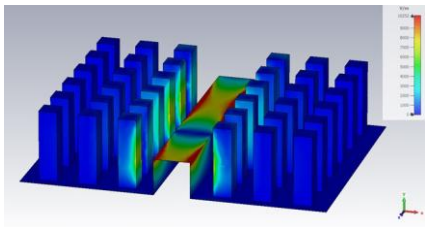

Fig. 4. Electric field distribution in the RGW with a reduced ridge height of h_{ridge} = 3 mm.

Table 1. Change of the cutoff frequency with the ridge height

Ridge height (mm)	5.75	5	3	2
f_c (GHz)	9.96	10.65	14.43	17.27

Finally, we have performed the MP analysis of a finite section of this waveguide (the simulated results have been obtained for standard aluminium SEY data from [26], compiled in Table 2) with the software tool SPARK3D. Fig. 5 shows the obtained MP power threshold P_{TH} of this RGW (h_{ridge} = 5.38 mm) from 17 to 18 GHz. For the requested simulations, the driving EM fields have been computed with CST Studio Suite. Fig. 5 confirms that the initial RGW is

suitable for performing MP measurements in the selected facility (since the P_{TH} values are consistently below 6.8 kW, i.e., they remain within the 7 kW limit of the available laboratory equipment).

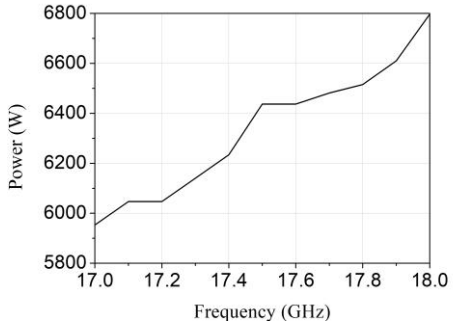

Fig. 5. P_{TH} computed with SPARK3D for a section of the initial RGW in the 17-18 GHz frequency range.

Table 2. Standard SEY data for aluminium (Al) material

Material	***E_max (eV)***	***E1 (eV)***	δ_0	δ_{max}
Al (ECSS2020 [26])	276	17.0	0.8	2.92

III. PARAMETRIC STUDY OF MP IN THE RGW

Starting from the initial RGW designed in section II, and in order to know the sensitivity of this RGW in terms of MP breakdown to variations of its geometry, a complete parametric study has been done. We have performed an analysis of the obtained MP power threshold P_{TH} of such waveguide when varying its fundamental design parameters (the ridge width a_{ridge} and height h_{ridge}, and also the distance between the ridge and the bed of pins p -see Fig. 1-) at the frequency of 17.5 GHz. In all cases, it has been checked that, for the frequency band of interest (from 17 to 18 GHz), the RGW works in monomode regime (only the ridge mode propagates), and that the region of maximum EM field level is mainly located over the ridge and not over the metallic pins, as stated in section II.

In Fig. 6(a) the obtained P_{TH} levels in the RGW as a function of the ridge width a_{ridge} are represented (starting from a_{ridge} = 3 mm, i.e., the value for the initial design obtained in section II), for different values of the ridge height h_{ridge}. Each curve corresponds to a different value of h_{ridge} (all of them fulfilling the required conditions of monomode regime and fields concentrated around the ridge), keeping the distance of the ridge to the bed of pins to p = 1.1625 mm (corresponding to the value of the initial design). The parametric study of the dependence of the P_{TH} with the ridge parameters reveals that decreasing the ridge height of the RGW has a significant impact on the threshold power required for a multipactor electron discharge to occur, as can be seen in Fig. 6(a). Specifically, the smaller the gap between the ridge and the top metal lid, the lower the power required for an electron discharge to occur in the RGW. On the other hand, when the ridge width increases, it is observed that the threshold power remains relatively stable at certain values (except a light increasing tendency for the shorter ridge value, h_{ridge} = 4 mm). These observations suggest that the ridge width will not be a critical parameter in terms of threshold power, while the ridge height will play a determining role when reducing the gap between the ridge and the top metal lid.

Furthermore, it is interesting to study the behaviour of the RGW in terms of P_{TH} when varying the distance between the bed of pins and the central ridge, as can be seen in Fig. 6(b), while keeping the remaining parameters equal to those in the initial RGW configuration. This figure reveals that the distance between the central ridge and the bed of pins is not a relevant parameter in terms of the threshold power that the RGW can support, given that we can observe a small variation of threshold levels for different values of this parameter. Additionally, this parameter is not a relevant factor in terms of single-mode propagation. It is important to note that, for all analyzed cases, the multipactor discharge occurred in the central area over the ridge.

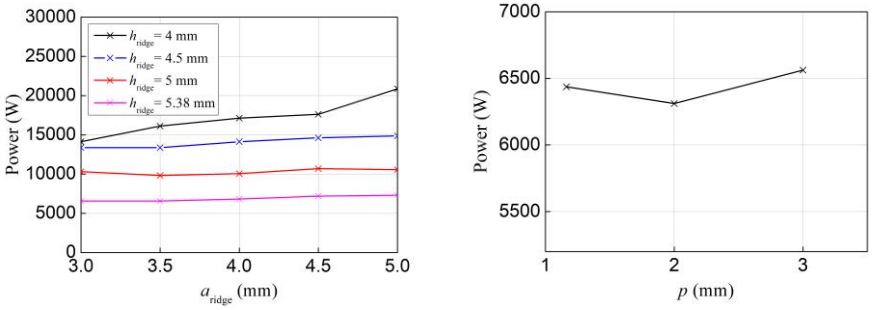

(a) (b)

Fig. 6. (a) P_{TH} in the RGW as a function of the ridge width a_{ridge} for different values of the ridge height h_{ridge}. (b) P_{TH} depending on the distance between the ridge and pin bed.

The most important conclusions to highlight about the performed parametric study can be summarized as follows: the ridge width is not a relevant factor in terms of the multipactor threshold power of the RGW. This allows for a good margin and degree of freedom when designing a RGW. It is important to remember that this is a key factor in components designs, as the variation of the width is usually employed to control the characteristic impedance of the line. On the other hand, it has a minimal impact on the single-mode propagation frequency range. Similar to the width, the distance between the central ridge and the bed of pins (p) has minimal impact on the MP threshold power level it can support (see Fig. 6(b)), as we observed only minor variations in this value when varying the p parameter significantly. Once again, it is not a relevant factor in terms of single-mode propagation, and this insensitivity is convenient for practical designs with bends or corners, where keeping a constant distance between pins and ridge is not always possible. However, the ridge height is the most relevant parameter in terms of power handling in the design of RGW, affecting in a very direct way, and in practice, inversely proportional to the multipactor threshold power level that can support the RGW. It has been proved that the higher the ridge height, the lower the multipactor threshold power, since the gap between the two metallic surfaces, ridge and top lid, is smaller and more prone to hold an electron discharge in this area.

IV. TRANSFORMER DESIGN

All the conclusions extracted in the previous section have been obtained based on theoretical considerations, simulations performed in the selected RGW through electromagnetic field computations, and multipactor modeling software using perfect conductor material (thus minimizing insertion losses). Now, in order to fully validate these results, a RGW prototype will be fabricated and measured in the future. After that, the corresponding multipactor test will be carried out. However, to be able to perform multipactor tests in the available high power laboratory, the designed RGW will need to be connected to standard rectangular waveguide ports. Thus, it is essential to design a matching stage, consisting of an impedance transformer from the standard waveguide to the designed RGW.

In particular, as the multipactor test of the RGW prototype will be done in the frequency band of 17-18 GHz, we will use the standard *WR-51* as a waveguide port (E, $b_{WR\text{-}51}$ = 6.477 mm), whose monomode operation frequency range is located between 15 and 22 GHz. On the other hand, given that at the operating frequency band of 17-18 GHz the maximum measurable power in the laboratory is about 6.5 - 7 kW, the transformer has been designed for a RGW with the following parameters: a_{ridge} = 3 mm, h_{ridge} = h_{pin} = 5.75 mm, d =3.25 mm, h_A = 0.727 mm, p = 1.625 mm. Finally, it has been checked that the P_{TH} obtained in this final RGW design (with this new ridge height value), within the frequency band of 17–18 GHz, does not exceed the maximum measurable power level. The ridge height is increased from 5.38 mm (initial value) to 5.75 mm, as there was almost no margin before reaching the maximum measurable multipactor power threshold level in the laboratory. Increasing the ridge height, the multipactor threshold decreases and we make sure that the power level can be measured. It is also important to note that after including the impedance transformer, P_{TH} levels may slightly differ, as will be shown next.

The impedance transformer will consist of a set of ridge steps in gap waveguide technology arranged consecutively, whose ridges will be decreasing in width and increasing in height, since the standard *WR-51* waveguide is significantly wider than the designed RGW and without ridges. Therefore, as can be seen in the scheme of one half of the designed transformer in Fig. 7 (where the bed of pins is not shown for simplicity), we will start from an initial ridge block almost as wide as the width of the *WR-51* and with a small height. Then, the following blocks will be narrowing and increasing in height gradually until reaching the last block, whose ridge will have dimensions very close to the height and width values of the designed RGW ridge.

Our impedance transformer will be based on an initial model of 7 steps progressively decreasing from the initial ridge of our RGW (in blue in Fig. 7) to the standard *WR-51* waveguide (with no ridge and thus not shown). The dimensions of the 6 intermediate ridges given in Fig. 7, whose final values for matching a RGW with a length of 6

periodic cells (i.e., with 6 metallic pins along the propagation direction) are given in Table 3. They have been determined after an optimization process performed in CST Studio Suite.

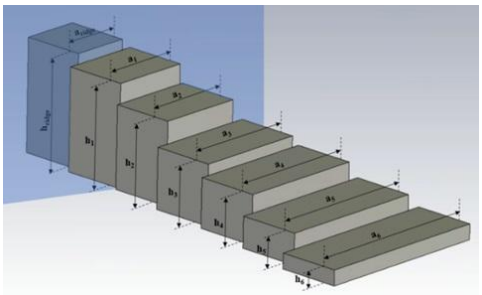

Fig. 7. Scheme of one half of the designed transformer (without the bed of pins) with the ridge height and width dimensions.

Table 3. Final values of the steps height and width in the final designed transformer

A1	A2	A3	A4	A5	A6
4.0175	4.3682	5.5276	6.6214	7.5696	9.5103
B1	B2	B3	B4	B5	B6
5.2121	4.2474	3.0450	2.4469	1.5423	0.8499

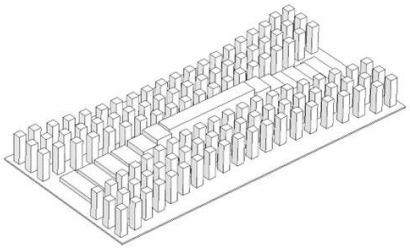

Fig. 8. Scheme of the complete transformer with the center section of our RGW.

Fig. 8 shows the scheme of the complete RGW to *WR-51* waveguide transformer with the centre section of our RGW, while its simulated electrical response is displayed in Fig. 9 (here metal losses of aluminium have been considered). Although the RGW has been specifically designed for operation in the 17-18 GHz frequency band, the RGW to *WR-51* waveguide transformer has been optimized for a wider frequency band, which extends from 15.5 to 20.5 GHz. In this frequency range, the return losses are higher than 20 dB, and the insertion losses are lower than 1 dB, thus revealing a good matching between both waveguides (see results in Fig. 9).

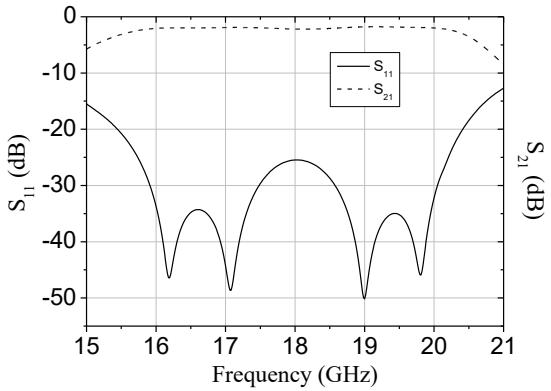

Fig. 9. Simulated electrical response of the designed RGW to *WR-51* waveguide transformer.

Once the final prototype of the impedance transformer has been designed and electrically characterized, we have performed the high-power study through a MP analysis with SPARK3D. In particular, all the high-power simulations performed have shown that the discharge electron clouds are always located in the RGW (central area of the transformer) and above the ridge (see, for example, the electron cloud distribution shown in Fig. 10 for an RF input power of 4.3 kW at 17 GHz). The calculated P_{TH} values in the designed RGW including transformers (back-to-back

configuration) are represented in Fig. 11. As can be checked, these values are below the maximum power that can be measured in the laboratory (about 6.5 - 7 kW) for the considered frequency range, as expected from the same MP analysis that was also performed for this RGW without the transformers (see Fig. 11).

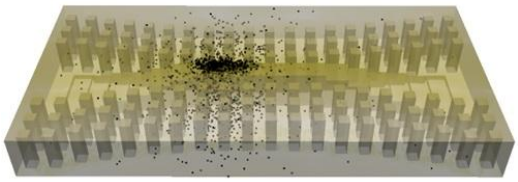

Fig. 10. Electron cloud distribution of a multipactor discharge (RF input power of 4.3 kW at 17 GHz) inside the transformer.

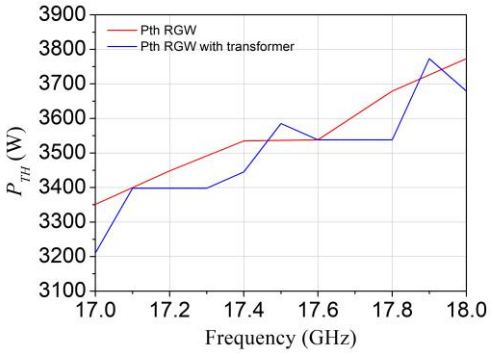

Fig. 11. Comparison of the calculated P_{TH} in the final designed RGW (h_{ridge} = 5.75 mm) with and without transformers (back-to-back configuration).

V. CONCLUSION

In this work, a theoretical study of the multipactor effect in RGW technology has been performed. For this purpose, simulated results (using a commercial software tool) of the dependence of multipactor power threshold on various parameters, such as the ridge dimensions and its proximity to the bed of pins are considered. This study reveals that, in terms of power handling, the most relevant parameter in the RGW under study is the ridge height, so the higher the ridge height (for a fixed gap), the lower the multipactor threshold power that supports the RGW. On the other hand, the rest of RGW parameters (the ridge width, the distance from the ridge to the bed of pins and the pins parameters) are not relevant in terms of the multipactor threshold power of the RGW, so we can afford a good margin and degree of freedom when designing a RGW. These conclusions are relevant for practical designs, as it is common practice when designing devices with RGW to adjust the ridge width to achieve different impedances, while the distance to the bed of pins is not always kept constant due to bends or corners present in most components. Therefore, the insensitivity of the multipactor threshold to these two parameters is important for microwave engineers. On the other hand, the dependence on ridge height is a factor that must be considered. In most existing designs, the ridge height is assumed to be identical to the height of the surrounding pins to simplify the manufacturing process. However, the gap between the pins and the top lid is typically kept quite small to increase the bandgap provided by the pins, which can compromise the multipactor threshold. In principle, the ridge height can be chosen to be lower than that of the pins without affecting waveguide performance. Thus, the conclusions from this study are crucial to be considered when addressing space-related applications using this novel guided technology.

ACKNOWLEDGMENT

The authors would like to thank ESA and VSC, for contributing with its installations—cofunded by the European Regional Development Fund—a way of making Europe [24].

REFERENCES

[1] J. R. M. Vaughan, “Multipactor,” *IEEE Trans. Electron Devices*, vol. ED-35, no. 7, pp. 1172–1180, July 1988.
[2] M. Jiménez, B. Gimeno, C. Miquel-Espanya, D. Raboso, S. Anza, C. Vicente, J. Gil, F. Quesada, Á. Alvarez, M. Taroncher, M. Reglero, and V. E. Boria, “Analysis of the electromagnetic radiation generated by a multipactor

discharge occurring within a microwave passive component," *J. Phys. D: Appl. Phys.*, vol. 43, no. 39, p. 395501, October 2010.
[3] A. J. Hatch and H. B. Williams, "The secondary electron resonance mechanism of low-pressure high-frequency gas breakdown," *J. Appl. Phys.*, vol. 25, no. 4, pp. 417–423, April 1954.
[4] A. Wood and J. Petit, "Diagnostic investigations into the multipactor effect, susceptibility zone measurements and parameters affecting a discharge," *ESA/ESTEC*, Noordwijk, The Netherlands, Work. Paper 1556, November 1989.
[5] A. Coves, G. Torregrosa-Penalva, C. P. Vicente, A. M. Pérez, B. Gimeno, and V. E. Boria, "Time evolution of an electron discharge in a parallel-plate dielectric-loaded waveguide," *IEEE Trans. Electron Devices*, vol. 55, no. 9, pp. 2505–2511, September 2008.
[6] G. Torregrosa-Penalva, A. Coves, B. Gimeno, I. Montero, C. Vicente, and V. E. Boria, "Multipactor susceptibility charts of a parallel-plate dielectric-loaded waveguide," *IEEE Trans. Electron Devices*, vol. 57, no. 5, pp. 1160–1166, May 2010.
[7] V. E. Semenov, E. I. Rakova, D. Anderson, M. Lisak, and J. Puech, "Multipactor in rectangular waveguides," *Phys. Plasmas*, vol. 14, no. 3, p. 033501, March 2007.
[8] C. Vicente, M. Mattes, D. Wolk, B. Mottet, H. L. Hartnagel, J. R. Mosig, and D. Raboso, "Multipactor breakdown prediction in rectangular waveguide based components," in *Proc. IEEE MTT-S Int. Microw. Symp. Dig.*, Long Beach, CA, USA, June 2005, pp. 1055–1058.
[9] E. Chojnacki, "Simulations of a multipactor-inhibited waveguide geometry," *Phys. Rev. Special Topics Accel. Beams*, vol. 3, no. 3, p. 032001, March 2000.
[10] A. Berenguer, Á. Coves, F. Mesa, E. Bronchalo, and B. Gimeno, "Analysis of multipactor effect in a partially dielectric-loaded rectangular waveguide," *IEEE Trans. Plasma Sci.*, vol. 47, no. 1, pp. 2687–2697, January 2019.
[11] A. M. Pérez, V. E. Boria, B. Gimeno, S. Anza, C. Vicente, and J. Gil, "Multipactor analysis in circular waveguides," *J. Electromagn. Waves Appl.*, vol. 23, no. 11–12, pp. 1575–1583, 2009.
[12] A. Frotanpour, B. Gimeno, and S. Esfandiarpour, "Multipactor in dualmode elliptical waveguide," in *Proc. 31st Int. Rev. Prog. Appl. Comput. Electromagn. (ACES)*, Williamsburg, VA, USA, May 2015, pp. 1–2.
[13] A. M. Pérez, V. E. Boria, C. Tienda, C. Vicente, S. Anza, J. Gil, B. Gimeno, and D. Raboso, "Prediction of multipactor breakdown thresholds in coaxial transmission lines for traveling, standing, and mixed waves," *IEEE Trans. Plasma Sci.*, vol. 37, no. 10, pp. 2031–2040, October 2009.
[14] D. González-Iglesias, O. Monerris, B. G. Martínez, M. E. Díaz, V. E. Boria, and P. Martín-Iglesias, "Multipactor RF breakdown in coaxial transmission lines with digitally modulated signals," *IEEE Trans. Electron Devices*, vol. 63, no. 10, pp. 4096–4103, October 2016.
[15] V. E. Semenov, E. I. Rakova, A. G. Sazontov, I. M. Nefedov, V. I. Pozdnyakova, I. A. Shereshevskii, D. Anderson, M. Lisak, and J. Puech, "Simulations of multipactor thresholds in shielded microstrip lines," *J. Phys. D: Appl. Phys.*, vol. 42, no. 20, p. 205204, September 2009.
[16] J. J. Vague, I. Asensio, Á. Coves, Á. A. San Blas, M. Reglero, A. Vidal, D. Raboso, M. Baquero-Escudero, and V. E. Boria, "Study of the multipactor effect in groove gap waveguide technology," *IEEE Trans. Microw. Theory Techn.*, vol. 70, no. 5, pp. 2566–2578, May 2022.
[17] P. S. Kildal, E. Alfonso, A. Valero-Nogueira, and E. Rajo-Iglesias, "Local metamaterial-based waveguides in gaps between parallel metal plates," *IEEE Antennas Wireless Propag. Lett.*, vol. 8, pp. 84–87, 2009.
[18] E. Rajo-Iglesias and P. S. Kildal, "Numerical studies of bandwidth of parallel-plate cut-off realised by a bed of nails, corrugations and mushroom-type electromagnetic bandgap for use in gap waveguides," *IET Microw. Antennas Propag.*, vol. 5, no. 3, pp. 282–289, February 2011.
[19] P. Kildal, A. Zaman, and E. Rajo-Iglesias, "Design and experimental verification of ridge gap waveguides in bed of nails for parallel plate mode suppression," *IET Microw. Antennas Propag.*, vol. 5, no. 3, pp. 262–270, February 2011.
[20] F. Fan, J. Yang, V. Vassilev, and A. U. Zaman, "Bandwidth investigation on half-height pin in ridge gap waveguide," *IEEE Trans. Microw. Theory Techn.*, vol. 66, no. 1, pp. 100–108, January 2018.
[21] E. Alfonso, M. Baquero, P. Kildal, A. Valero-Nogueira, E. Rajo-Iglesias, and J. I. Herranz, "Design of microwave circuits in ridge-gap waveguide technology," in *Proc. 2010 IEEE MTT-S Int. Microw. Symp.*, Anaheim, CA, USA, 2010, pp. 1–1.
[22] E. Rajo-Iglesias, M. Ferrando-Rocher, and A. U. Zaman, "Gap waveguide technology for millimeter-wave antenna systems," *IEEE Commun. Mag.*, vol. 56, no. 7, pp. 14–20, July 2018.
[23] A. Farahbakhsh, D. Zarifi, and A. U. Zaman, "A mmWave wideband slot array antenna based on ridge gap waveguide with 30% bandwidth," *IEEE Trans. Antennas Propag.*, vol. 66, no. 2, pp. 1008–1013, February 2018.
[24] European Space Agency (ESA) and Val Space Consortium (VSC) High-Power Laboratories, Valencia, Spain. [Online]. Available: www.val-space.com
[25] CST Studio Suite, version 2023, Dassault Systèmes, 2023.
[26] "Multipacting and Design Test," European Cooperation for Space Standarization (ECSS), ESA-ESTEC, ESA Publication Division, The Netherlands, Rep. ECSS-E-ST-20-01C, June 2020.